10-24-2016

Collapse Resistance of Moment Resisting Frame and Shear Wall RC Structural Systems Exposed to Blast

Alaa I. Chehab
Wayne State University, alaa.chehab@wayne.edu

Christopher D. Eamon
Wayne State University, eamon@eng.wayne.edu

Joshua Griffin
Kimley-Horn, josh.griffin@kimley-horn.com

Collapse Resistance of Moment Resisting Frame and Shear Wall RC Structural Systems Exposed to Blast

Alaa I. Chehab, A.M.ASCE[1]; Christopher D. Eamon, M.ASCE[2]; and Joshua Griffin[3]

Abstract

Various characteristics of a structure influence its response when subjected to a blast load. This has important implications for survivability and resistance to progressive collapse. In this study, the effect of the type of lateral load resisting system on reinforced concrete building resistance to progressive collapse when exposed to blast load is examined. Fourteen different reinforced concrete structures were considered for analysis, with five structures designed as moment resisting frames and nine designed as shear walls systems. Buildings with 3, 6, and 10 stories with 3, 4, and 5-bay symmetric configurations were considered. The structures were exposed to external and internal charges, while the nonlinear, transient dynamic analysis of collapse behavior was investigated with a finite element based approach, the applied element method (AEM). The results show that the shear wall structures and structures larger in height and plan generally provide greatest resistance to blast damage and progressive collapse.

Keywords: RC structures; Progressive collapse; FEM; AEM; Shear walls; Blast Loads.

[1] Ph.D. Candidate, Dept. of Civil and Environmental Engineering, Wayne State University, Detroit, MI 48202. E-mail: alaa.chehab@wayne.edu

[2] Associate Professor, Dept. of Civil and Environmental Engineering, Wayne State University. E-mail: eamon@eng.wayne.edu

[3] Structural Engineer, Kimley-Horn, Raleigh, NC 27601. E-mail: josh.griffin@kimley-horn.com

Introduction

Progressive collapse refers to the phenomenon where failure of a structural component causes or contributes to the collapse of adjoining members, which then causes additional collapse of the structure (GSA 2003). Since the events of 9-11, various research studies have been undertaken to further examine extreme load events and to suggest how corresponding damage may be mitigated. From these efforts, several analyses and design guidelines to improve structure resistance to progressive collapse have been developed (ASCE 2010; GSA 2003; USDOD 2005). Of the research work available, some focused specifically on modeling the World Trade Center events (Bazant and Zhou 2002; Wierzbicki and Teng 2003; Lynn and Isobe 2007), while others evaluated the effectiveness of different blast modeling approaches in general (Powell 2005; Li and Shi 2008). Approaching this issue from a probabilistic perspective and considering the interaction of other extreme loads, Asprone et al. (2010) proposed a probabilistic model for multi-hazard risk associated with the limit state of collapse for a generic four story reinforced concrete structure, subjected to blast in the presence of seismic risk. Later, Málaga-Chuquitaype et al. (2016) investigated the influence of secondary frames on the mitigation of collapse in steel structures subjected to earthquake and blast scenarios, as well as localized fire and blast hazards.

A larger number of research efforts studied idealized buildings of steel or reinforced concrete from a deterministic approach. Among the existing studies of steel moment frame structures, Grierson et al. (2005), Zhang et al. (2010) and later Korol et al. (2011), presented a progressive collapse analysis, while Hamburger and Whittaker (2004) found that frames might resist collapse by redistributing loads to adjacent columns. The performance of steel braced frames that were subjected to sudden removal of a first story column was investigated by Kim et al. (2008), while a similar analysis was presented by Gross and McGuire (1983). Alashker and El-Tawil (2011) discussed the use of calibrated macro-models to model progressive collapse, and a design-oriented model was proposed for computing the load resisting capacity of composite steel-concrete floors subjected to interior column loss. They concluded that the macro and micro models produced similar collapse response.

Various studies considered the analysis of reinforced concrete structures as well. Nonlinear pushover analyses (nonlinear static procedure) of reinforced concrete walls coupled by steel beams have been discussed (El-Tawil et al. 2002). Several investigated the behavior of the structure when exposed to an explosion near ground level (Almusallam et al. 2010; Xu and Liu 2009), while Sasani et al. (2011) used experimental data and analytical results to evaluate the progressive collapse resistance of an actual building that followed severe initial damage. Rather than simulate an explosion, others simply instantaneously removed ground floor columns to study the potential effect of severe damage (Sasani and Sagiroglu 2008; Hong et al. 2006).

The studies above provide a relatively small but significant body of knowledge regarding progressive collapse under extreme blast load events. Although both steel and reinforced concrete structures were considered, the existing research has been limited to moment resisting and braced frame buildings, whereas structures that use shear walls for lateral load resistance have not been considered in detail. However, this type of system may in fact display a significantly different performance when exposed to blast loads than frame-type buildings. For example, on January 25, 1971, while under construction, the floor slabs of the 16 story 2000 Commonwealth Avenue building in Boston, MA failed, resulting in a progressive collapse of approximately 60% of the building. However, the progressive failure stopped at the location of the shear walls surrounding the elevator core, saving the remaining portion of the building

(Granger et al. 1971). This type of behavior is generally not seen with similar moment frame and braced frame buildings. However, the typical differences in behavior for these structures exposed to blast loads are currently not well quantified. Thus, the objective of this study is to investigate the difference in progressive collapse performance between a selection of reinforced concrete structures with shear walls systems and corresponding structures with moment resisting frames when exposed to blast loads.

Structures Considered

Two sets of hypothetical structures were designed according to American Concrete Institute (ACI) 318-11 Code Standards, where one set was designed to resist the lateral loads using a moment resisting frame (MRF), and the other using a shear wall system. The buildings were assumed to be located in Detroit, Michigan, and design loads were determined according to ASCE 7-10 for office building occupancy, resulting in a dead to live load ratio of approximately 1.5:1. As load combinations involving seismic loads were found not to govern, wind loads were used for lateral design and were determined with the directional procedure. As no special seismic detailing was required, the structures were designed as ordinary moment frames and shear walls that satisfied general ACI 318 reinforcing requirements for continuity and structural integrity. Three building geometries were considered for analysis; symmetric 10 story structures with either 3x3, 4x4, or 5x5 bays, where all columns are spaced at 6.1 m. Additional 4x4 structures of 3 and 6 stories were also designed to examine the effect of building height, as discussed below. In all structures, the first floor height is taken as 4.3 m and the remaining floor heights are 3.7 m, with slab thickness of 180-200 mm. Slab reinforcement is taken as #5 (15.8 mm) bars with 25.4 mm cover. Columns are 355 (3 story buildings), 460 (6 story buildings), and 560 mm (10 story buildings) square and are taken to have fixed supports on the ground floor. As necessary to meet code strength requirements, total column longitudinal reinforcement area varied, where #6 (19 mm), #7 (22.2 mm), or #8 (25.4 mm) bars were used with 50 mm cover. Stirrups consisted of #3 (9.5 mm) bars. Shear wall thickness is taken as 300 mm with #4 (12.7 mm), #5 (15.8 mm), or #8 (25.4 mm) reinforcing bars, as required, with 50 mm cover. Concrete strength is taken as 28 MPa, while reinforcing steel yield strength is taken as 414 MPa. The resulting structures are shown in Fig. 1, where column and shear wall locations are indicated on the top floor.

Numerical Model

Structures were modeled with the fully nonlinear, large strain, large displacement finite element-based blast analysis code ELS, which is described elsewhere (ASI 2010; Meguro & Tagel-Din 2002). With the approach implemented in ELS, the 'applied element method'(AEM), elements are connected by a series of springs on element surfaces, where one normal and two shear springs (one in each direction) are located at each surface contact point, as shown in Fig. 2-a. Spring stiffness varies as a function of stress or strain as given by the material model, and once a specified failure criterion is reached, as discussed below, the springs release element connectivity, which allows efficient simulation of material softening and fracture along element lines. When contact occurs between elements, linear springs are generated at contact points to transfer energy between elements.

For concrete, the Maekawa elasto-plastic and fracture model (Maekawa and Okamura 1983) is implemented, as shown in Fig. 2-b. In this model, Young's modulus, the fracture parameter (which defines the extent of existing damage, as a function of the load history), and the current plastic strain are used to define the compressive stresses-strain relationship. Although represented simply as a uniaxial stress-strain relationship in Figure 2-b for illustration, the softening behavior of the concrete is governed by the resulting multi-axial stress state caused by the combination of normal and deviatoric stresses imposed on the element. That is, the state of stress and resulting damage caused by an interaction of axial, shear, and flexural deformations are implicitly accounted for in the model. For the 27.6 MPa compressive strength (f'_c) concrete considered, modulus of rupture (f_r) was taken as 2.6 MPa and modulus of elasticity as 24,800 MPa, while shear modulus (*G*) was taken as 9,650 MPa. These material properties are summarized in Table 1. When concrete is subjected to tension, stiffness is taken as the initial stiffness until the cracking point is reached, at which point the effected spring(s) joining adjacent concrete elements are released. If separated element surfaces contact, the connective springs are regenerated (with zero tension strength). This unloading and reloading behavior is illustrated in Fig. 2-b. Shear behavior is considered linear until cracking strain (as calculated from principle stress) is reached.

Strain rate strengthening is frequently accounted for by imposing an empirically developed curve that adjusts strength based on rate of strain (see, for example, Eamon et al. 2004). However, in AEM, an alternative approach was implemented. In this method, Poisson's ratio is lowered to zero under high strain rates, preventing the lateral expansion of the material and corresponding creation of lateral cracks (i.e. element separation), essentially strengthening the material under high rates of strain. As detailed by Tagel-Din (2009), this approach was shown to have good agreement to the traditional strain rate curve approach as well as to experimental data.

Steel reinforcing bars are modeled explicitly with spring (i.e. bar) elements, in which the nonlinear stress-strain response described by Ristic et al. (1986) governs behavior (Fig. 2-c). Tangent stiffness is calculated based on the state of strain, loading/unloading status and the previous load history, which controls Bauschinger's effect, where rupture is reached once the normal stress is equal to or greater than the ultimate stress of the steel material. The yield and ultimate stresses for steel reinforcement were taken as f_y = 414 MPa and f_u = 538 MPa, respectively. The steel modulus of elasticity was set equal to 200,000 MPa, with shear modulus of 11,000 MPa. Steel material properties are summarized in Table 1.

Often in practice, constraints related to the project schedule, budget, or available computational resources may not allow the blast event and its corresponding pressure-time history to be directly modeled. As such, it is common practice to simply remove a member from the structure to simulate its loss of load-carrying capacity under blast. As noted above, although some studies simulated blast effects in this manner and loaded the resulting structure only with gravity loads, initial analyses conducted for this study found significant differences in structural response between column removal and failing the same column with blast pressure. Specifically, for several structures it was found that a complete collapse resulted when a blast pressure was applied, while no collapse resulted when the same columns were simply removed. In these cases, this difference occurred because the blast load also damaged members near the removed columns as well, significantly weakening the adjoining beams and slab in some cases. Using an assumed spherical (i.e. non-directional) blast charge, it was generally found to be very difficult, if not impossible, to apply sufficient blast pressure that would remove the members of interest, but yet leave adjacent members relatively undamaged from the blast. Therefore, all collapse analyses for this study were initiated using blast pressure. Here, a simplified blast model was used where blast pressures resulting from a spherical TNT charge are calculated using the free-field wave equation based on TM5-1300 (Departments of the Army, Navy, and Air Force 1990). The explosion was taken as an unconfined surface burst, since the detonations were located outdoors and close to the ground (taken approximately 1 m above ground in all analyses), so that the initial shock is amplified at the point of detonation due to the ground reflection. In this case, where the charge height (Z_c) is less than twice the charge radius (R_c), the charge radius is calculated for a spherical shape as:

$$R_c = \sqrt[3]{3w / 4\Pi\rho_{TNT}} \quad (1)$$

where the charge weight (w) is multiplied by a magnification factor,

$$M_f = 2.0 - Z_c / 0.5R_c \quad (2)$$

Here, the TNT charge density (ρ_{TNT}) is taken as 1650 kg/m^3. The air is considered an ideal gas at sea level and the atmospheric pressure $(P_a) = 101{,}325$ Pascal. Based on the charge weights selected (see below), an external blast effect sufficient to cause two adjacent ground floor columns to fail in each model was considered. This was found to be equivalent TNT weights of approximately 340, 590 and 700 kg for the 3, 6, and 10 story buildings, respectively. That is, all structures of the same height, both shear wall and MRF, were exposed to the same charge weight for consistent comparison. This resulted in nearly all of the structures considered (10 story) being exposed to the same equivalent TNT weight of 700 kg. However, for the two 3 and 6 story structures considered, charge weights were reduced because the initial 700 kg charge would have resulted in complete destruction of these smaller buildings, due to their substantially lower column capacities, and no difference in performance between MRF and shear wall buildings would be obtainable. It should be noted that the use of different charge weights for these smaller buildings likely corresponds to a different probability of occurrence than for the larger charge weight applied to the 10 story structures, and thus comparisons of safety cannot directly be made between structures of different heights. In this blast model, blast pressures are applied to element surfaces that have a direct line of sight with the TNT charge. It should be noted that the main purpose of the blast analysis was to produce an extreme load that allows reasonable comparison of the response of different structures to possible progressive collapse, rather than to simulate the blast event itself in great detail. Thus, to ease numerical implementation of the comparison, various blast load simplifications were implemented. In particular, the effects of temperature, suction pressure, blast wave reflections on the structure, explosive casing (bare TNT weight only considered), and possible ground motion were neglected. Moreover, all structures are assumed to have a nonstructural façade that is destroyed upon blast impact, before significant additional pressure can be distributed to the structural system. In accordance to the recommendations in USDOD 2002, during the blast load event, the service dead load and 50% of the service live load were applied to the models as lumped masses added to the slabs.

The resulting models ranged in size from approximately 55,000-117,000 rectangular solid elements, and were solved using a time step increment of 0.0001 s during the blast stage. For the first two levels of the models, element edge lengths varied from 9-12 cm for columns, 14-20 cm for beams, and 18-30 cm on slabs. For the upper stories, a more coarse mesh was used, with element sizes approximately doubled. Similarly, wall element dimensions ranged from 15-37 cm. It was found that the use of a finer mesh resulted in differences in localized fracture patterns, but produced no significant differences in global response, the concern of this study, and thus was not computationally justified. That is, since in the AEM approach, as cracks may only develop and propagate along element boundaries, increasing the number of elements may result in the development of different crack patterns. For example, in some cases, increasing element density results in a larger number of smaller cracks as opposed to a small number of large cracks. Although several alternative crack patterns may sufficiently capture component behavior to accurately model the response of the overall structure, as was found in this study, the crack pattern that results from a more coarse mesh may be insufficient to model phenomenon at a smaller scale (crack geometry, local damage pattern on the component, accurate assessments of curvature and deflected shape, etc.)

A smaller time step increment of 0.00001 s was also considered, and was found to produce slightly larger force effects on the structure during the blast stage. However, it was determined that the excessive additional computational effort required for this smaller time step was similarly not justified for this study, as relative differences in performance between the different structures considered were unchanged. Each analysis required approximately 32-54 hours of CPU time on a 2.3-GHz quad-core CPU with 8 GB of RAM.

Verification Cases

Experimental verification of the collapse behavior of full-scale, actual buildings subjected to blast is challenging, as few experimental subjects exist. However, in this study, for validation, the analysis approach was used to model the progressive collapse of two actual reinforced concrete buildings subjected to explosive demolition. These structures are the Crabtree Sheraton Hotel located at Raleigh, NC (May, 2006) and Stubbs Tower located at Savannah, GA (December, 2007), for which the structural plans and demolition video footage were obtained. The Crabtree Sheraton Hotel was a 10-story (30 m high) building in a 3 x 9 bay rectangular plan configuration (total plan dimensions 18 m x 36 m) with a two-way flat plate floor system (1800 mm thick). The Stubbs Tower was a 15 story (45 m high) building constructed using two types of loadbearing systems; a column and girder concrete frame system for the first floor and load bearing concrete walls for the remaining floors. The building was structured in a 3 x 16 bay configuration (19 m x 56 m total plan dimensions). Both structures were modeled using the numerical technique discussed above. It was found that the analytical simulations well-matched the progressive collapse behavior of both structures, as shown in Figs. 3 and 4. In Fig. 4, vertical displacements were measured from the available video footage of the collapses at the points (*V*) as indicated in Fig. 3. Therefore, the method was considered sufficiently accurate for the modeling purposes of this study. Other researchers have had similar success with the AEM approach for modeling collapse behavior as well (Kernicky et al. 2014; Salem et al. 2014; Salem 2011; Keys and Clubley 2013; Lupoae et al. 2013).

Results

Moment Resisting Frame Structures

As the objective of the study is to compare the collapse behavior of different structures subjected to a similar level of damage, for all external blast analyses, the charge position was selected such that two adjacent exterior columns just failed. For all structures, this was approximately 1 m away from the face of the structure, centered between the two central columns, as shown in Fig. 5. With the charge in this position, approximately four seconds after the blast, the 3x3 MRF structure experienced a complete progressive collapse, as shown in Fig. 6. Note that, beyond 4.0 s (not shown), all floors of the structure eventually collapsed to the ground.

As shown in Fig. 6, the blast first resulted in collapse of the floor slab in the bay adjacent to the charge, which failed from the uplifting blast pressure. Next, the two columns closest to the blast (C2 and C3 in Fig. 7) failed in bending caused by the blast pressure as well as a large increase in moment caused by the axial gravity loads, which became increasingly eccentric to the deformed column mid-section. Once these columns failed, the remaining columns quickly followed. Studying the changes in column forces as a function of time, as shown in Fig. 8, it can be seen that columns C6 and C7 were also directly affected by and failed in bending from the blast pressure, at a slightly delayed time, while columns C1, C4, C5 and C8 failed primarily in compression (actually due to combined compressive and bending effects, but axial compression was greatly dominant) due to redistribution of the gravity loads. This is evident at t=0.3 s in Fig. 8, where the axial loads in these columns greatly increased once columns C2, C3, C6, and C7 lost axial load carrying capacity (i.e. where axial force becomes approximately 0 at t=0.4 s in Fig. 8). Note that, the design axial capacity (nominal capacity reduced by the appropriate resistance factor) for exterior columns C1, C4, C5, and C8 is approximately 4,497 kN, while maximum axial loads on these columns varied from 1,780 kN to 4,890 kN at any time in the analysis. However, the interior columns (C6, C7, C10, and C11) have higher design axial capacities of approximately 4,640 kN. Thus, although columns C10 and C11 carried larger amounts of (redistributed) axial load (Fig. 7 at t=2.05 s) they did not fail first because their axial capacity is higher than the adjacent exterior columns.

The failure times for columns C5, C1, C4, and C8 occurred approximately at 1.2 s, 1.85 s, 2.05 s, and 2.2 s, respectively, as shown in Fig. 8, where large, abrupt decreases in axial force in the column occurs. These failure times correspond to the times for which the axial force diagrams are constructed in Fig. 7. An examination of column moments indicates that bending moment was not a main reason for the failure of most columns (exceptions: C2, C3, C6, and C7, which were closest to the blast), since the moment capacity was generally not exceeded in the analysis. For example, for columns C1, C4, C5, and C8, the moment capacity is approximately 270 kN-m, while maximum moments on these columns did not exceed 136 kN-m during the analysis.

For the corresponding 4x4 MRF structure, approximately 2.5 s after charge detonation, a major progressive collapse occurred, as shown in Fig. 9-c. The collapse behavior for the 4x4 and 3x3 MRF structures was similar, where axial loads carried by damaged columns nearest to the blast were redistributed to the remaining columns, causing progression of the collapse.

Considering the 5x5 MRF structure, approximately 4 s after charge detonation, severe local damage near the blast location occurred (slab and column failure), but the structure did not collapse, as shown in Fig. 10. Similar to the 3x3 structure, once a local failure occurred, a more extensive redistribution of axial loads followed throughout the 5x5 frame due to the greater number of available members. Although the members furthest away from the blast received relatively little load, this surrounding structural system was an important influence on overall system behavior. These surrounding members not only reduced the redistributed axial loads further, but also provided additional constraint and stability for the most heavily loaded portions of the structure, preventing progressive collapse.

In this structure, the time-displacement curve of a point at the top of the most severely damaged column (C3) shows that the maximum downward vertical (Z) displacement was approximately 127 mm at t=2.9 s. After t=2.9 s, no significant additional vertical displacement occurred, as shown in Fig. 10. The horizontal displacement in the direction parallel to the blast direction (X) shows the structure vibrating with a period of approximately 1.5-2 s, while the horizontal displacement perpendicular to the blast (Y) shows no significant motion after column C3 failed (due to blast). These small changes in horizontal and vertical displacements after the failure of Columns C2, C3 and C4 indicate the sustained stability of the structure. Columns just adjacent to the failed columns (C2, C3 and C4) carried the majority of the redistributed axial forces from the failed columns, but as noted above, the larger number of members surrounding the damaged columns allowed for successful load redistribution and continuing stability. Overall, as expected, the analyses of the three MRF structures indicate that increasing the number of bays results in a more successful redistribution of axial loads over the remaining stable structure components once a local collapse has been initiated.

Shear Wall Structures

For the 3x3 shear wall structure, after running the analysis for approximately 5.0 s, a major progressive collapse resulted. However, the remaining shear wall core remained stable, as shown in Fig. 11.

The axial forces carried by the major structural components are given in Fig. 12. As shown, the shear walls carry approximately 54% (27,179 kN) of the total axial load (50,265 kN) at t=2.0 s. Clearly, they have a significant influence on axial force distribution. During the analysis, columns C1, C2, C3, and C4 failed first, then, as shown in Fig. 13, the failure of columns C6 and C7 occurred simultaneously with the partial failure of shear wall S1 at approximately t=1.8 s (due to direct blast pressure). The failure of these components then increased the axial loads on the remaining shear walls S2, S3 and S4, which occurs at approximately t=1.8 s in Fig. 13. At approximately t=2.5 s, the impact of the falling slabs with the damaged shear wall S1 (Fig. 11) caused a large increase in the axial force in shear wall S3 as S1 failed completely, while simultaneously, shear walls S2 and S4 experienced a large decrease in axial force, as shown in Fig. 13. This occurs because the impact of the floor slabs into the shear wall tower was accompanied by a large lateral (impact) load. Conceptually, after the failure of S1, the remaining shear wall structure acted similar to a cantilever beam, fixed at ground level, with a U-shape in section, where S3 acted as the compression flange and S2 and S4 as the tension webs. However, the remaining shear walls remained stable after t=5.0 s in the analysis, since the failure of the slabs also resulted in removal of the axial loads that they had previously transferred to the shear walls.

For the 4x4 shear wall structure, in approximately 4.5 s, a progressive collapse of about 50% of the structure occurred, but the collapse stopped at the location of the shear walls. Here, the shear walls provided the structure with significant stability, as shown in Fig. 14. In this structure, the floor slabs in the bays adjacent to the charge first failed from the uplifting blast pressure. Simultaneously, the closest columns to the charge (C1-C4 and C7) failed in bending caused by the blast pressure. Once these exterior columns failed, the floor slabs which they supported toppled onto adjacent first floor columns, causing their failure (see t=2.5 s in Fig. 14). However, progressive collapse of the floor slabs was halted at the location of the shear walls, preventing failure of the remaining columns.

In addition, the shear walls were able to carry a significant portion of the axial load that was previously carried by the damaged columns. The axial force curves in Fig. 15 show how the shear walls (S1, S2, S3 and S4) and the columns (C8, C12, C14 and C18) at the ends of the shear walls shared the axial loads in a way that reduced excessive axial loads on these columns. For example, from t=0.3 s to approximately t=0.75 s, as the structure sways, we can observe that S1, S4, C8 and C12 (Group 1) are subjected to an increase in axial loads, while S2, S3, C14 and C18 (Group 2) are subjected to a decrease in axial loads. This behavior is reversed after t=0.75 s, where Group 1 components are subjected to a decrease in axial loads, while Group 2 components are subjected to an increase in axial loads. Clearly, the columns and shear walls act efficiently together as two distinct groups of components, sharing the axial loads. The sway of the shear wall core can be seen more clearly in Fig. 16, where walls and columns facing the blast (walls S1, S4 and columns C8, C12) have highest compression at the times when walls and columns opposite the blast (walls S2, S3 and columns C14, C18) have lowest compression.

For the 5x5 shear wall structure, although a collapse began upon detonation, similar to the other shear wall structures, the progressive collapse stopped at the shear walls, as shown in Fig. 18-b (at t=5.0 s). The behavior of the shear walls of the 5x5 model was very similar to that of the shear walls of the 4x4 model. In both models, the walls carried a significant amount of axial load, which reduced the magnitude of the redistributed axial loads to the columns adjacent to those that failed. This resulted in halting the progression of the collapse. Moreover, a secondary effect of the presence of the shear walls is that they contributed significantly to aid in blocking falling debris and slabs from striking and damaging the remaining stable components of the structure.

Effect of Building Height

To examine the effect of building height on collapse performance, the 4x4 structure was redesigned with 3 and 6 story configurations, where column and shear wall capacities were altered as discussed above. It was found that as building height decreased, overall collapse behavior was similar to that of the 10 story structures, as shown in Figs. 9, 17-a, and 17-b. However, the charge weight needed to fail two exterior columns, and correspondingly initiate collapse, decreased for the lower height buildings. For the 3 story building, a charge weight of 340 kg, approximately half that needed to initiate collapse of the 10 story building, resulted in total collapse. For the 6 story building, a charge weight of 590 kg was required to initiate collapse. Such results are not unexpected, since ground floor column capacity decreases with decreasing building height. Quantitatively, it was found that the ratio of charge weights needed to fail the different height structures fell within the ratio of column capacities for axial force and moment. Specifically, for the 6 story building, the ratios of: a) column nominal axial capacity to that of the 3 story structure, followed by b) charge weight needed to fail the buildings, and c) column nominal moment capacities, are: (1.2, 1.7, 3.0). Similarly, ratios for the 10 story to the 3 story structure are: (1.8, 2.1, 3.6).

It should also be noted that as height increased, a slight delay in the collapse progression occurred. As shown in Figs. 9, 14, and 17, the rate of collapse progression was highest and lowest for the three and ten story structures, respectively. For example, in Fig. 9, two stories of the 3 story structure partially collapsed at the same time (1.5 s) that 1 story of the 6 story structure and no stories in the 10 story structure partially collapsed.

Effect of Shear Wall Location

To study the effect of shear wall location, two additional configurations were considered for the 4x4 and 5x5 10 story structures. These additional configurations explored the effect of moving the shear walls from the original central location to progressively more dispersed arrangements. As shown in Figs. 17-c and 17-d (compared to Fig. 14), for the 4x4 structure, changing shear wall arrangement had minimal effect on overall behavior, as in each case, collapse of a significant portion of the structure resulted. As shown, it was also found that separating the shear walls resulted in failure of one of the walls closest to the blast. For the 5x5 structure, however, separating and moving the shear walls to the exterior of the building (which were placed perpendicular to the facade, to avoid blocking potential fenestration) resulted in greatly minimizing damage from the blast, and resisted system collapse (Fig. 18-c). Thus, it appears that shear wall placement may have a significant influence on collapse resistance, but the effect is highly dependent on building geometry and component strength. By consideration of shear wall and charge placement, the models were specifically constructed to locate the blast charge as far as possible from the shear walls, while attempting to maintain somewhat symmetric and reasonable wall placement schemes. This was done to minimize the potential shielding effect from the blast load that the shear walls may provide the columns, and also to minimize the beneficial effect of placing a high capacity structural element close to the blast source, which can more readily support the loads redistributed by failed columns. However, these effects cannot be eliminated completely, and are contributing factors to the performance of shear wall buildings. A secondary effect of the presence of the shear walls is that they contributed significantly to aid in blocking falling debris and slabs from striking and damaging the remaining stable components of the structure.

Effect of Charge Location

To study the effect of charge placement, the 10 story 4x4 structure was again considered. In this case, two additional analyses were conducted where the 700 kg charge that caused collapse when placed at the building exterior was progressively moved inward toward the center of the building. Charges were placed 1 m above the ground level, either 1 m from the center column or at the center of the corner bay of each structure, as shown in Fig. 19. For the MRF structures (Figs. 19-a and 19-b), changing charge location had no significant effect on behavior, where similar, complete collapse behavior resulted regardless of charge position. For the shear wall structure (Figs. 19-c and 19-d), moving the charge into the center of a corner bay resulted in a similar level of destruction as the original external charge location. However, when the charge was placed near the center of the building, insignificant damage to the structural system occurred. This is because the shear wall, although it experienced complete local removal of material by the blast, maintained sufficient resistance in the surrounding material to avoid collapse. Such a result suggests that a reasonably reinforced bearing wall structure has the potential to experience greater blast resistance than an equivalent frame structure.

Summary and Conclusions

In this study, the effect of the type of lateral load resisting system on reinforced concrete structure resistance to progressive collapse when exposed to blast load was examined using an existing finite element approach. The modeling technique employed was found to reasonably replicate the collapse behavior of two actual structures subjected to blast demolition for which data are available. Using this validated modeling approach, fourteen different reinforced concrete structures were considered for analysis, with five structures designed as moment resisting frames and nine designed as shear walls systems. Buildings with 3, 6, and 10 stories with 3, 4, and 5-bay symmetric configurations were considered. Charge weights required to fail two exterior columns in all structures varied from 340-700 kg, depending on building height, where lower height structures required the lower charge weights.

Under the blast loads considered, which were sized to just remove two exterior columns, the 10 story 3x3 and 4x4 MRF structures experienced complete collapse, while the 5x5 building suffered local damage only. In contrast, the performance of the shear wall buildings was dependent upon building size and shear wall placement. The 3x3 structure, with shear walls placed in the core of the building, resulted in complete collapse, with major damage to the shear walls. Regardless of shear wall placement, the 4x4 building experienced a partial collapse of approximately half of the structure, where the collapse progression halted at the shear walls. The 5x5 structure resulted in complete, partial, and no collapse, when shear walls were placed at the core, within middle bays, and within exterior bays of the structure, respectively.

Building height had little effect on overall performance once two exterior columns failed. All of the 3, 6, and 10 story MRF buildings resulted in complete collapse, while each of the 4x4 shear wall structures resulted in a partial collapse of approximately half of the building, which stopped at the location of the shear walls. Another parameter explored was blast location, where interior as well as exterior blasts resulted in complete collapse of the 4x4 MRF structure. However, a partial and no collapse resulted for the corresponding shear wall structure when the charge was placed within an exterior and a core bay, respectively.

Results for all analyses are summarized in Table 2, where the percent of collapsed floor area ("% collapsed") and the corresponding collapsed area per charge weight ("CA/TNT", in m^2/kg) are given. In the Table, models are designated with the bay configuration followed by height in stories, while labels "a", "b", and "c" refer to shear wall configurations as shown in Figs. 17-b, c, and d, respectively, for 4x4 models, and as shown in Figs. 18-a, b, and c, respectively, for 5x5 models. Finally, labels "i" and "e" refer to analyses where the charge was placed inside the structure, near the interior (i) and exterior (e), respectively, as shown in Fig. 19. Following the model label, the charge weight used is given in parenthesis (kg). As shown in Table 2, in terms of percent of floor area lost, all MRF structures except for the 5x5-10 model resulted in complete collapse, while none of the shear wall structures were fully destroyed. Although the range of destruction was large (from 1-96% collapsed), the average floor area loss was approximately 52%, with most values ranging from about 44-63%, substantially less than the typical 100% loss for corresponding MRF buildings. Correspondingly, average CA/TNT values were 5.3 for shear wall structures and 8.3 for MRFs, indicating that the MRFs were subjected to greater damage on an area lost per unit charge weight basis.

Of all parameters studied, in general, it was found that two were most significant on reducing potential for progressive collapse under blast loading; building size and shear wall placement. With regard to building size, as demonstrated in the analyses, larger structures carry two possible advantages. For building larger in plan, greater redundancy allows for increased load sharing ability among remaining structural members, potentially limiting surviving member overload and corresponding failure. For buildings larger in height, the associated increase in member capacities supply a larger capacity to resist blast load, requiring a larger charge weight to severely damage the structure. Moreover, as building plan as well as height increases, additional structural elements are available to allow bridging over damaged areas. With regard to shear wall placement, overall, it was found that moving the walls as close to the exterior bays as possible resulted in a greater resistance to progressive collapse. One reason for this is the associated increase in the moment of inertia of the building plan, allowing the structure as a whole to more effectively carry unbalanced axial loads caused by damaged columns. Here, with the exception of a shear wall destroyed by the blast, the progressive collapse generally stopped at the remaining shear walls.

Based on the results of this study, simply increasing first floor member capacities was found to be an effective way to significantly increase structural resistance to blast. As shown, for the structures considered, proportional increases of charge weight resisting ability roughly mirrored proportional increases in column strength. Along with increases in column strength, a larger building plan similarly demonstrated enhanced resistance to progressive collapse. Such construction might be justified architecturally by considering one large structure in favor of several smaller structures, for example. Second, the use of dispersed shear walls, where walls are placed in multiple locations near the building exterior, resulted in superior resistance to progressive collapse than placing shear walls at the building core. This approach, however, will likely cause tension between structural and architectural objectives, where one of the latter is generally to place shear walls inward near the building core. Additional consideration might be given to constructing a safe room for building occupants adjacent to a shear wall. The practice of placing stairwells within a shear wall core or adjacent to a shear wall may be ideal, allowing building occupants a stable passage of escape in the case of a blast emergency.

References

ACI (American Concrete Institute). (2011). “Building code requirements for structural concrete and commentary.” *ACI 318-11*, Farmington Hills, MI.

Alashker, Y., Li, H., and El-Tawil, S. (2011). "Approximations in progressive collapse modeling." J. Struct. Eng., 10.1061/ (ASCE) ST.1943-541X.0000452, 914-924.

Almusallam, T. H., Elsanadedy, H. M., Abbas, H., Alsayed, S. H., & Al-Salloum, Y. A. (2010). “Progressive collapse analysis of a RC building subjected to blast loads.” Structural Engineering and Mechanics, 36(3), 301-319.

ASCE (American Society of Civil Engineers). (2010), “Minimum design loads for buildings and other structures.” *SEI/ASCE 7-10*, Reston, Va.

Applied Science International (ASI), LLC. (2010). Applied Science International, Durham, North Carolina.

Asprone, D., Jalayer, F., Prota, A., & Manfredi, G. (2010). “Proposal of a probabilistic model for multi-hazard risk assessment of structures in seismic zones subjected to blast for the limit state of collapse.” Structural Safety, 32(1), 25-34.

Bažant, Z. and Zhou, Y. (2002). "Why did the world trade center collapse?—simple analysis." J. Eng. Mech., 10.1061/ (ASCE) 0733-9399(2002)128:1(2), 2-6.

Department of Defense (DOD). (2002). “DOD minimum antiterrorism standards for buildings”. Unified Facilities Criteria (UFC), UFC 4-010-01. U.S. Army Corps of Engineering, Washington, DC.

Department of Defense (DOD). (2005). “Design of buildings to resist progressive collapse.” Unified Facilities Criteria (UFC) 4-023-03.

Departments of the Army, the Navy, and the Air Force. (1990). “Structures to resist the effects of accidental explosions.” *TM5-1300*.

Eamon, C., Baylot, J., and O'Daniel, J. (2004). "Modeling concrete masonry walls subjected to explosive loads." J. Eng. Mech., 10.1061/ (ASCE) 0733-9399(2004)130:9(1098), 1098-1106.

El-Tawil, S. and Kuenzli, C. (2002). "Pushover of hybrid coupled walls. II: Analysis and behavior." J. Struct. Eng., 10.1061/ (ASCE) 0733-9445(2002)128:10(1282), 1282-1289.

General Services Administration (GSA), (2003), "Progressive collapse analysis and design guidelines for new federal office buildings and major modernization projects." Washington, DC.

Granger, R. O., Peirce, J. W., Protze, H. G., Tobin, J. J., & Lally, F. J. (1971). "The building collapse at 2000 Commonwealth Avenue, Boston, Massachusetts, on January 25, 1971." Rep. of the Mayor's Investigating Commission, Boston, Ma.

Grierson, D. E., Xu, L., & Liu, Y. (2005). "Progressive-failure analysis of buildings subjected to abnormal loading." Computer-Aided Civil and Infrastructure Engineering, 20(3), 155-171.

Gross, J. and McGuire, W. (1983). "Progressive collapse resistant design." J. Struct. Eng., 10.1061/ (ASCE) 0733-9445(1983)109:1(1), 1-15.

Hamburger, R., & Whittaker, A. (2004). "Design of steel structures for blast-related progressive collapse resistance." Modern Steel Construction, 44(3), 45-51.

Hong, H., Chengqing, W., Zhongxian, L., & AK, A. (2006). "Numerical analysis of structural progressive collapse to blast loads." Transactions of Tianjin University, S1.

Kernicky, T., Whelan, M., Weggel, D., and Rice, C. (2014). "Structural identification and damage characterization of a masonry infill wall in a full-scale building subjected to internal blast load." J. Struct. Eng., 10.1061/ (ASCE) ST.1943-541X.0001158, D4014013.

Keys, R. and Clubley, S. (2013). "Modeling debris distribution of masonry panels subject to blast loads using experimental & applied element methods." Proc., 15th International Symposium on Interaction of the Effects of Munitions (ISIEMS 15), Potsdam, DE, 17–20.

Kim, J. K., Lee, Y. H., & Choi, H. H. (2008). "Progressive collapse resisting capacity of braced frames." Journal of the Computational Structural Engineering Institute of Korea, 21(5), 429-437.

Korol, R. M., Sivakumaran, K. S., & Greening, F. R. (2011). "Collapse Time Analysis of Multi-Story Structural Steel Buildings." The Open Civil Engineering Journal, 5(1).

Li, Z., & Shi, Y. (2008). "Methods for progressive collapse analysis of building structures under blast and impact loads." Transactions of Tianjin University, 14, 329-339.

Lupoae, M., Baciu, C., & Constantin, D. (2013). "Theoretical and experimental research on progressive collapse of RC frame buildings." Urbanism. Arhitectur. Constructii, 4(3), 71-87.

Lynn, K. M., & Isobe, D. (2007). "Structural collapse analysis of framed structures under impact loads using ASI-Gauss finite element method." International Journal of Impact Engineering, 34(9), 1500-1516.

Maekawa, K., & Okamura, H. (1983). "The deformational behavior and constitutive equation of concrete using the elasto-plastic and fracture model." Journal of the Faculty of Engineering. University of Tokyo. Series B, 37(2), 253-328.

Málaga-Chuquitaype, C., Elghazouli, A. Y., & Enache, R. (2016). "Contribution of secondary frames to the mitigation of collapse in steel buildings subjected to extreme loads." Structure and Infrastructure Engineering, 12(1), 45-60.

Meguro, K. and Tagel-Din, H. (2001). "Applied element simulation of RC structures under cyclic loading." J. Struct. Eng., 10.1061/ (ASCE) 0733-9445(2001)127:11(1295), 1295-1305.

Powell, G. (2005). “Progressive collapse: Case studies using nonlinear analysis.” Proc., Metropolis & Beyond: Structures Congress and Forensic Engineering Symposium, New York, NY.

Ristic, D., Yamada, Y., & Iemura, H. (1986). “Stress-strain based modeling of hysteretic structures under earthquake induced bending and varying axial loads.” Research Rep. No. 86-ST, 1.

Salem, H. (2011). “Computer-aided design of framed reinforced concrete structures subjected to flood scouring.” Journal of American Science, 7(10), 191-200.

Salem, H., Mohssen, S., Kosa, K., & Hosoda, A. (2014). “Collapse analysis of Utatsu Ohashi Bridge damaged by Tohuku Tsunami using applied element method.” Journal of Advanced Concrete Technology, 12(10), 388-402.

Sasani, M., & Sagiroglu, S. (2008). “Progressive collapse of reinforced concrete structures: a multihazard perspective.” ACI Structural Journal, 105(1), 96.

Sasani, M., Kazemi, A., Sagiroglu, S., and Forest, S. (2011). "Progressive collapse resistance of an actual 11-story structure subjected to severe initial damage." J. Struct. Eng., 10.1061/ (ASCE) ST.1943-541X.0000418, 893-902

Tagel-din, H. (2009) “High fidelity modeling of building collapse with realistic visualization of resulting damage and debris using the applied element method.” Rep. No. HDTRA1-09-P-0006. Department of Defense.

Wierzbicki, T., & Teng, X. (2003). “How the airplane wing cut through the exterior columns of the World Trade Center.” International journal of impact engineering, 28(6), 601-625.

Xu, J. X., & Liu, X. L. (2009). “A two-step approach to progressive collapse analysis of building structures under blast loading.” Journal of Shanghai Jiaotong University (science), 14, 393-397.

Zhang, Y. M., Sun, C. J., Su, Y. P., & Su, J. Y. (2010). “Finite element analysis of vertical continuous collapse of six-story frame structure.” Applied Mechanics and Materials, 34, 1800-1803.

Xu, J. X., & Liu, X. L. (2009). “A two-step approach to progressive collapse analysis of building structures under blast loading.” Journal of shanghai jiaotong university (science), 14(4), 393-397.

Zhang, Y. M., Sun, C. J., Su, Y. P., & Su, J. Y. (2010). “Finite Element Analysis of Vertical Continuous Collapse of Six-Story Frame Structure.” Applied Mechanics and Materials, 34, 1800-1803.

List of Figures:

Table 1. Material Properties (MPa)

Material Property		Concrete	Steel
Compressive strength	f'_c	27.6	-
Modulus of rupture	f_r	2.6	-
Modulus of elasticity	E	24,800	200,000
Shear modulus	G	9,650	11,000
Yield stress	f_y	-	414
Ultimate stress	f_u	-	538

Table 2. Summary of Analysis Results

	Shear Wall		MRF	
Model	% collapsed	CA/TNT	% collapsed	CA/TNT
4x4-3 (340)	50	8.7	100	17.5
4x4-6 (590)	68	6.9	100	10.1
3x3-10 (700)	89	4.2	100	4.8
4x4-10.a (700)	50	4.2		
4x4-10.b (700)	63	5.3	100	8.5
4x4-10.c (700)	56	4.8		
5x5-10.a (700)	96	12.7		
5x5-10.b (700)	44	5.8	0.4	0.1
5x5-10.c (700)	16	2.1		
4x4-10.i (700)	0.6	0.1	100	8.5
4x4-10.e (700)	44	3.7	100	8.5

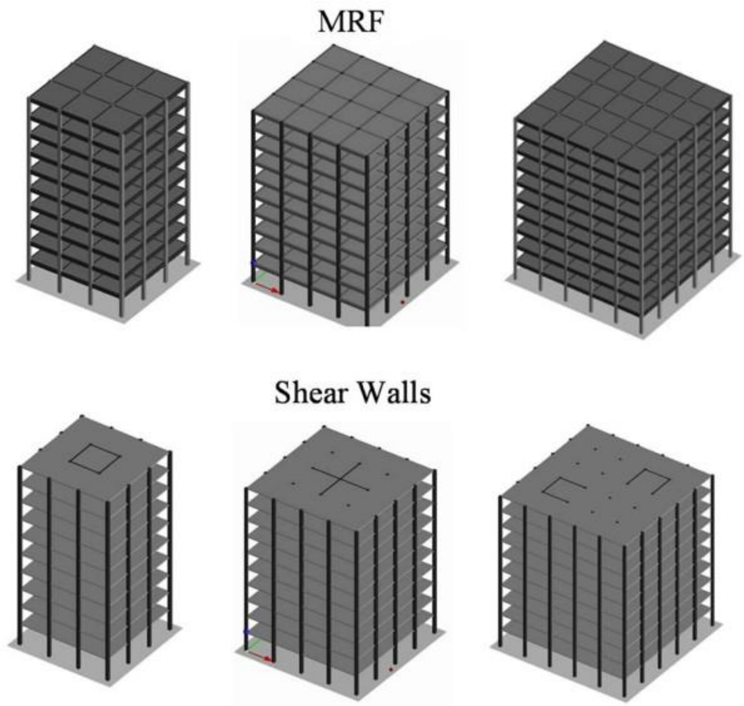

Fig. 1. Primary Ten Story Structures Considered for Analysis

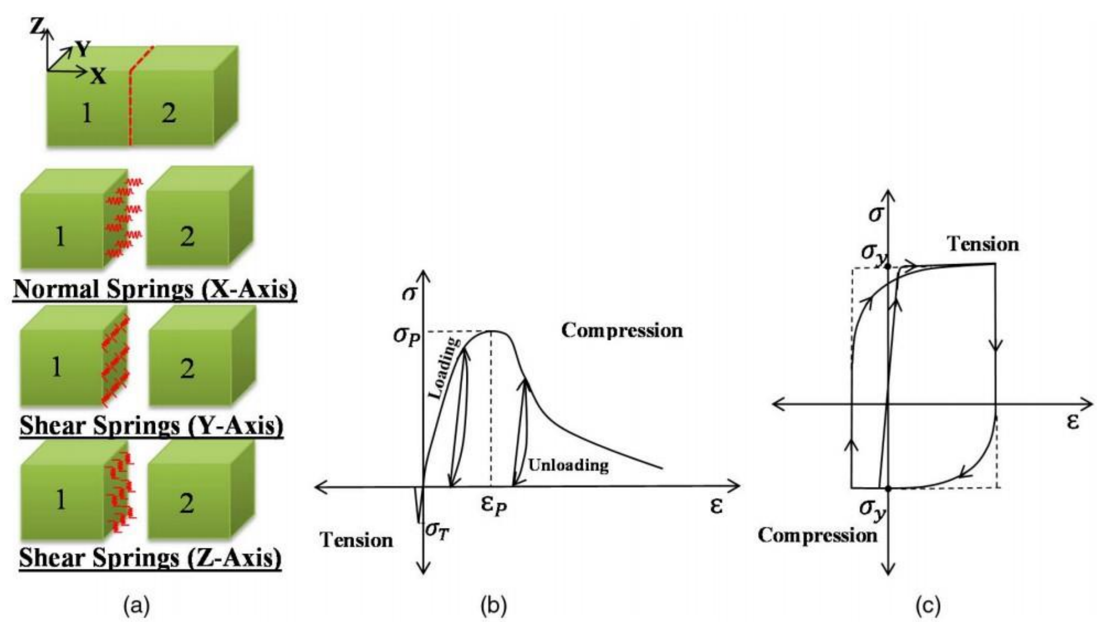

Fig. 2. (a) Concept of Element Connectivity Using AEM; (b) Concrete Model; (c) Steel Model

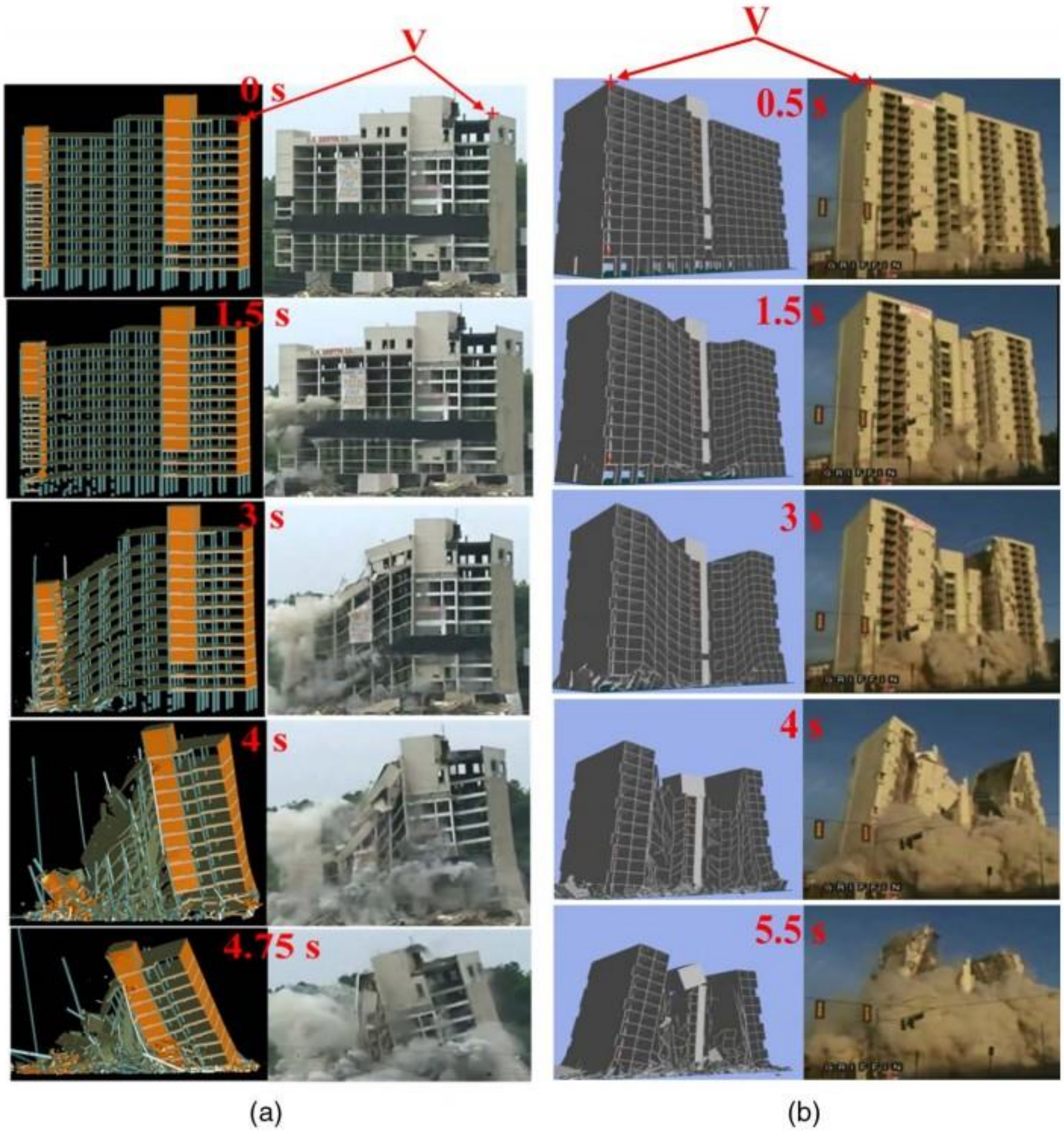

Fig. 3. Comparisons Between Actual Collapse Results and Simulation: (a) Crabtree Sheraton Hotel, Raleigh, NC; (b) Stubbs Tower, Savannah, GA

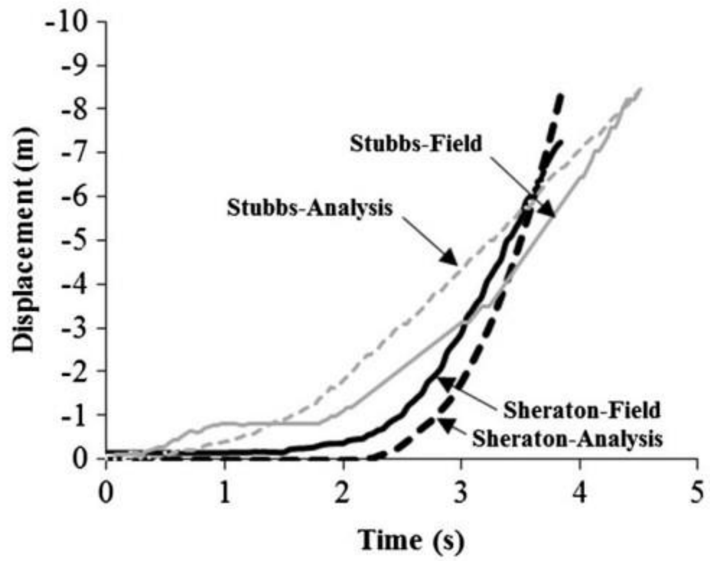

Fig. 4. Time-Displacement Response Comparison

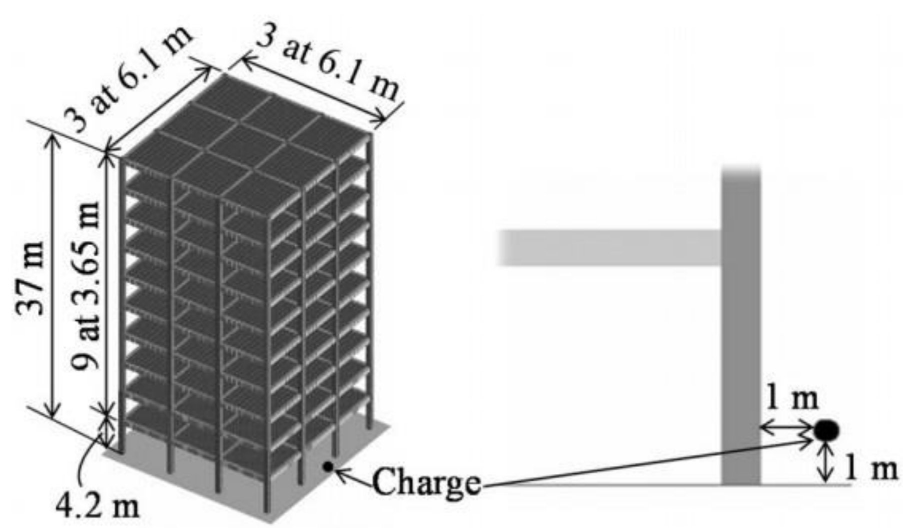

Fig. 5. Blast Analysis Configuration

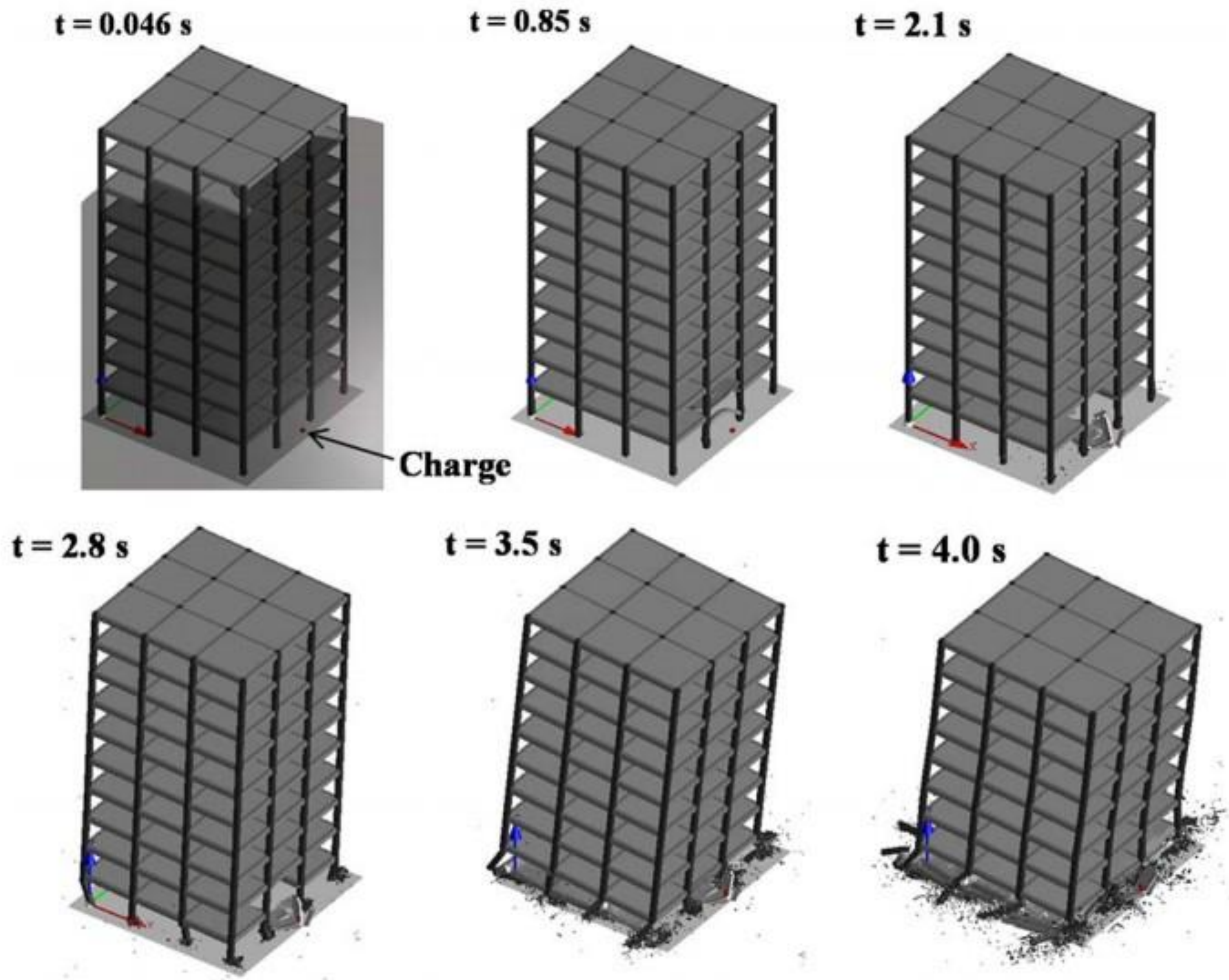

Fig. 6. Response of 3x3 MRF Structure

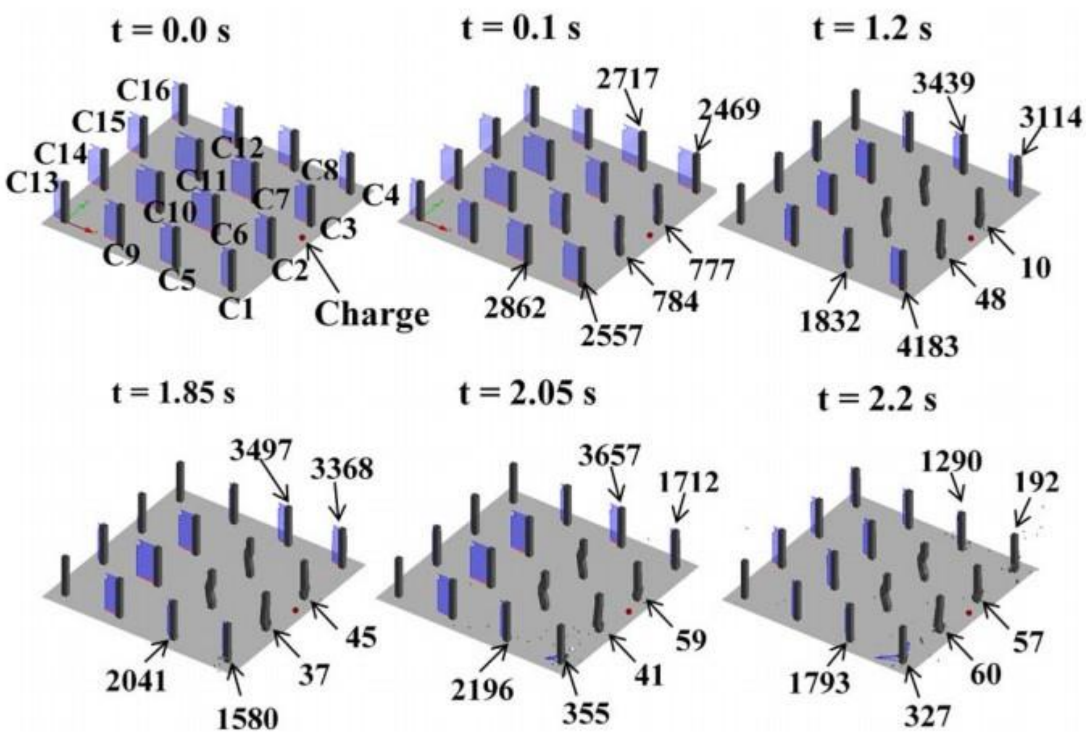

Fig. 7. First Floor Column Axial Forces (kN) for 3x3 MRF Structure

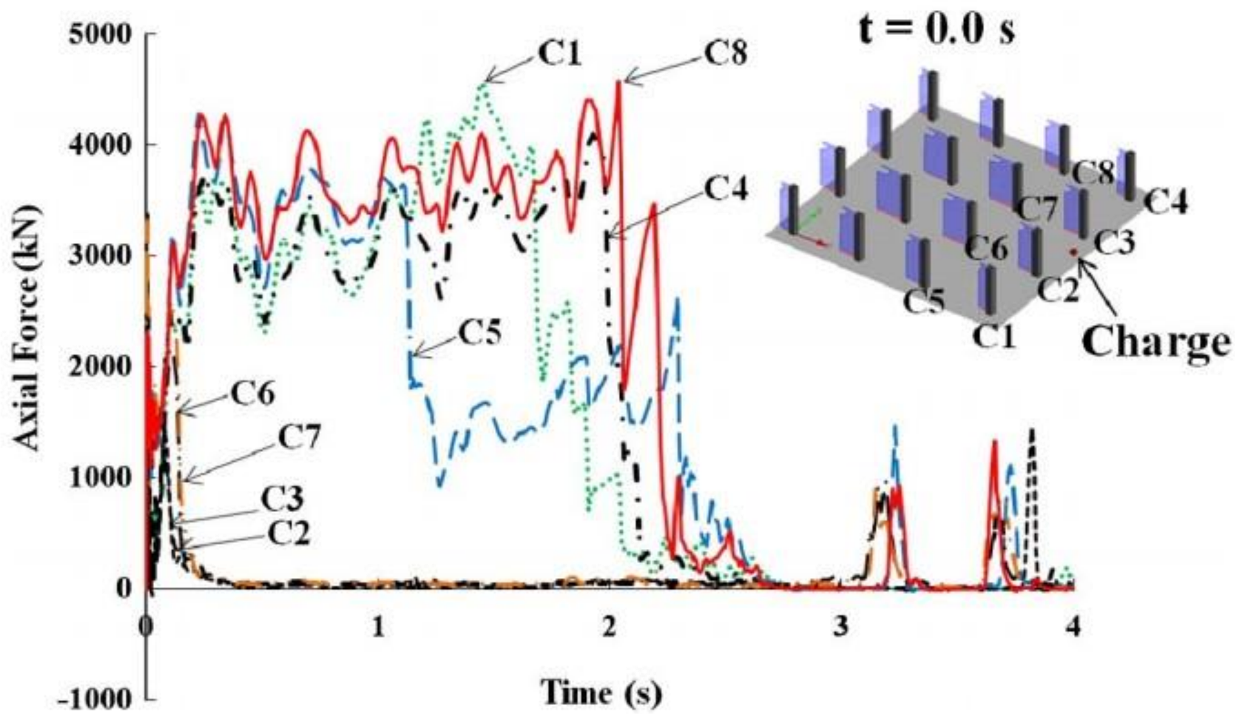

Fig. 8. Column Axial Forces as a Function of Time (3x3 MRF)

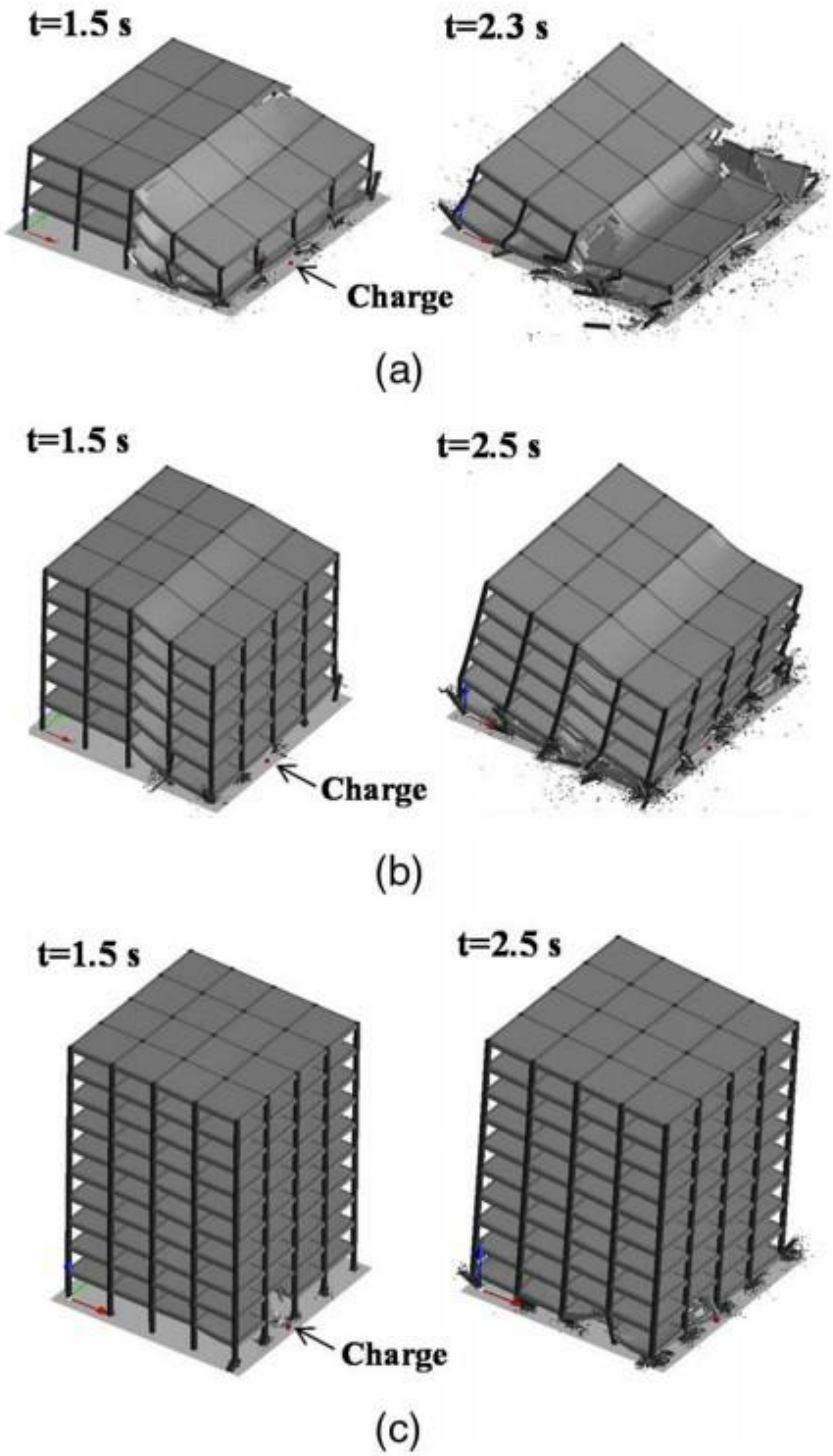

Fig. 9. Response of 4x4 MRF Structures: (a) 3 Stories; (b) 6 Stories; (c) 10 Stories

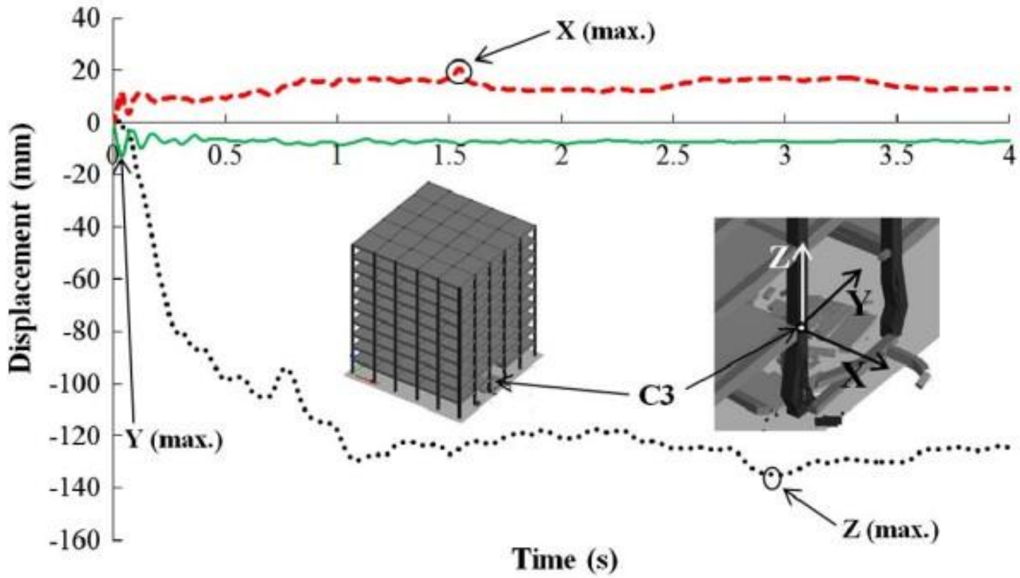

Fig. 10. Displacement at Top of Column C3 for the 5x5 MRF Structure

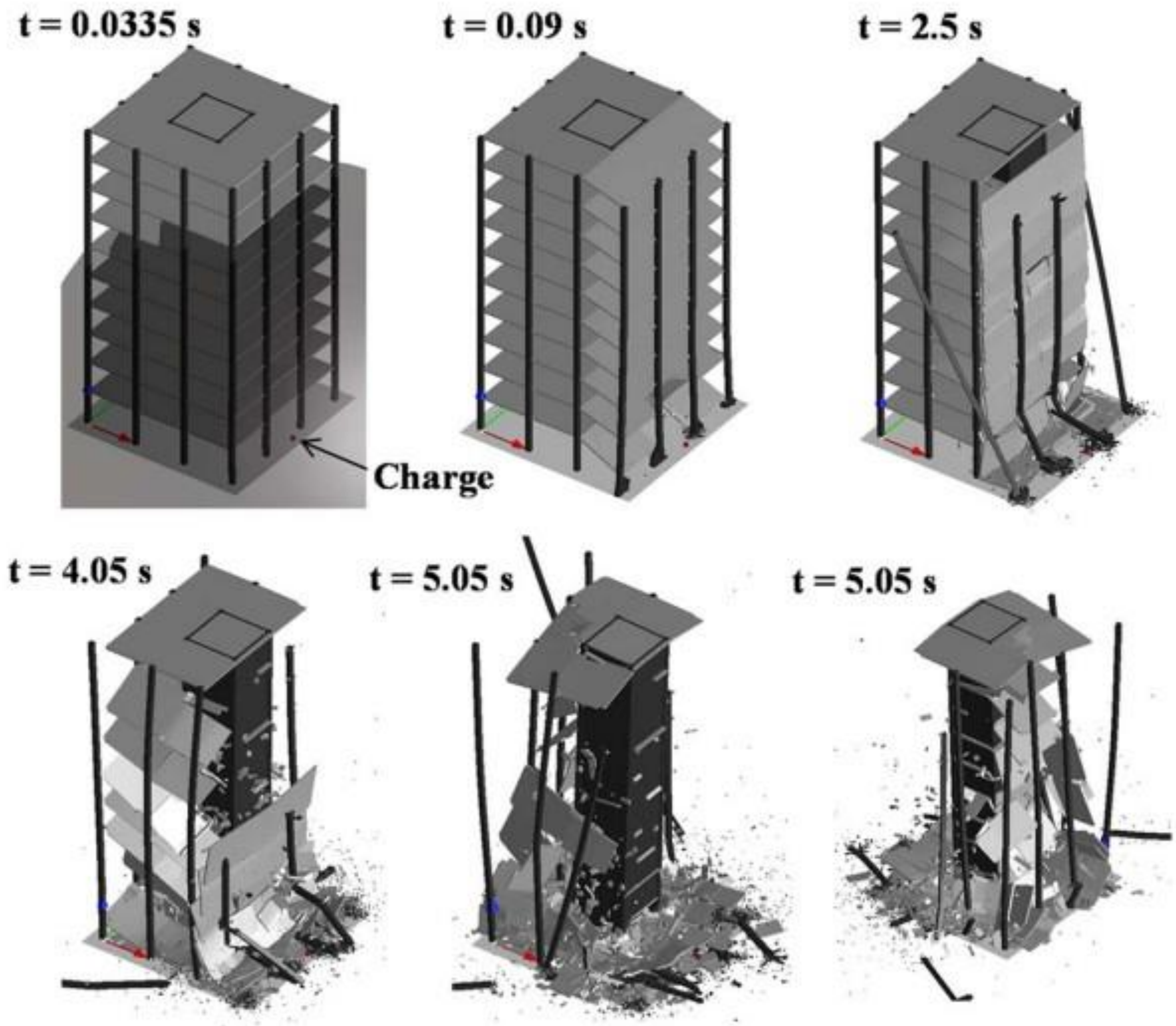

Fig. 11. Response of 3x3 Shear Wall Structure

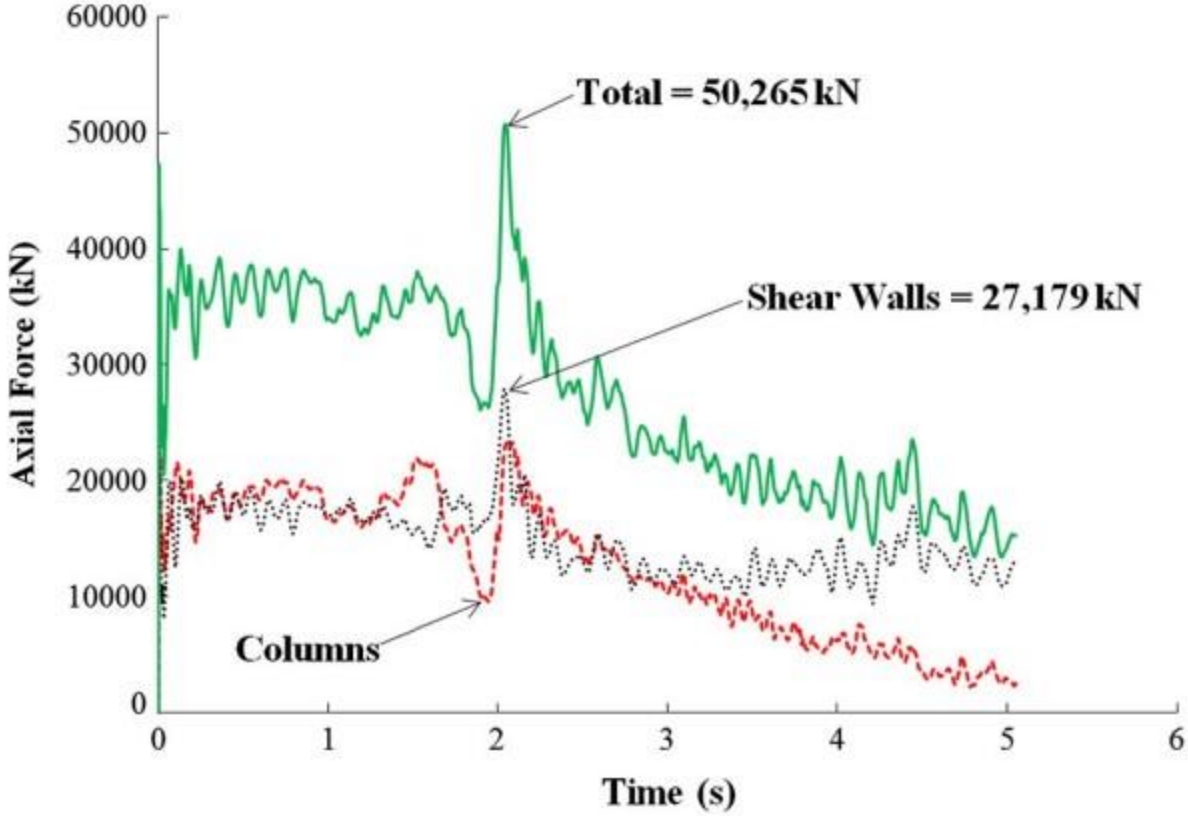

Fig. 12. Shear Wall Axial Load Contribution

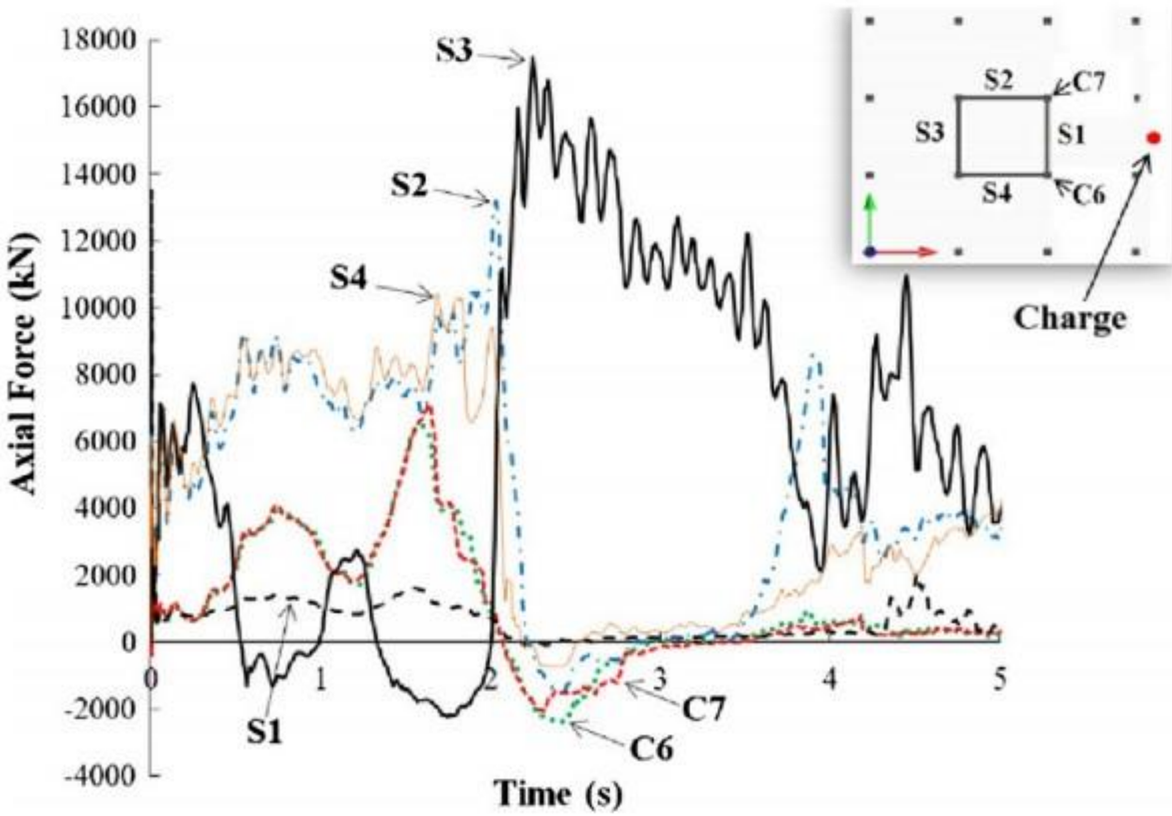

Fig. 13. Shear Wall and Column Axial Forces as a Function of Time (3x3 SW)

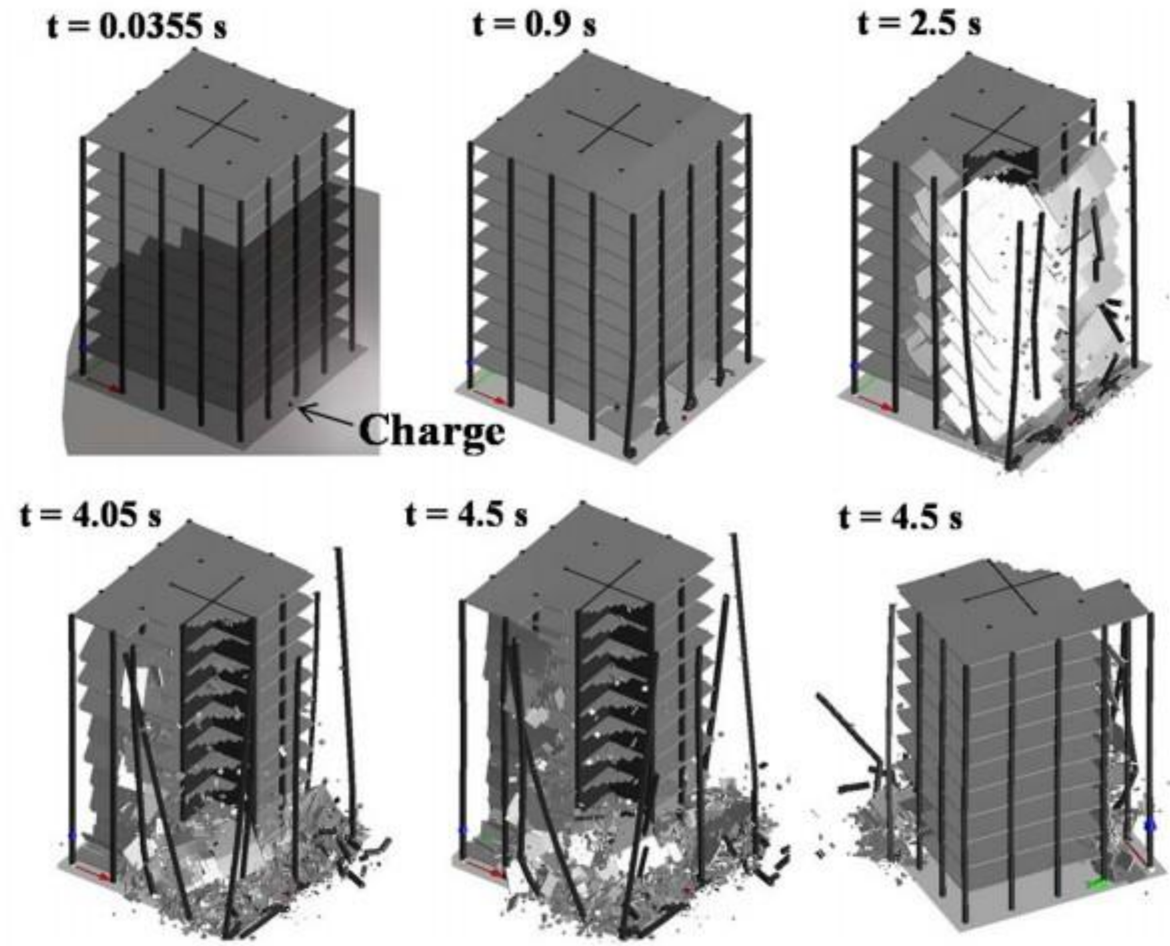

Fig. 14. Response of 4x4 Shear Wall Structure

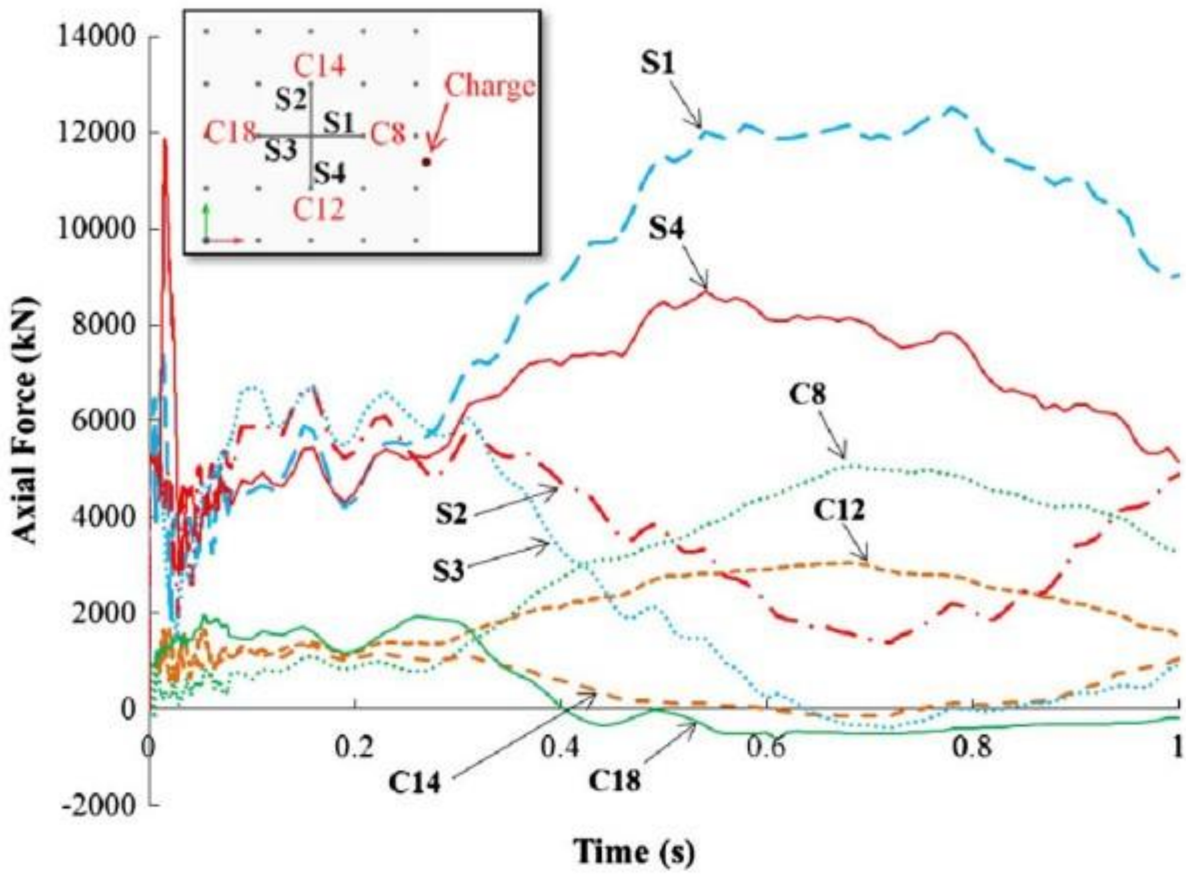

Fig. 15. Shear Wall and Column Axial Forces as a Function of Time (4x4 SW)

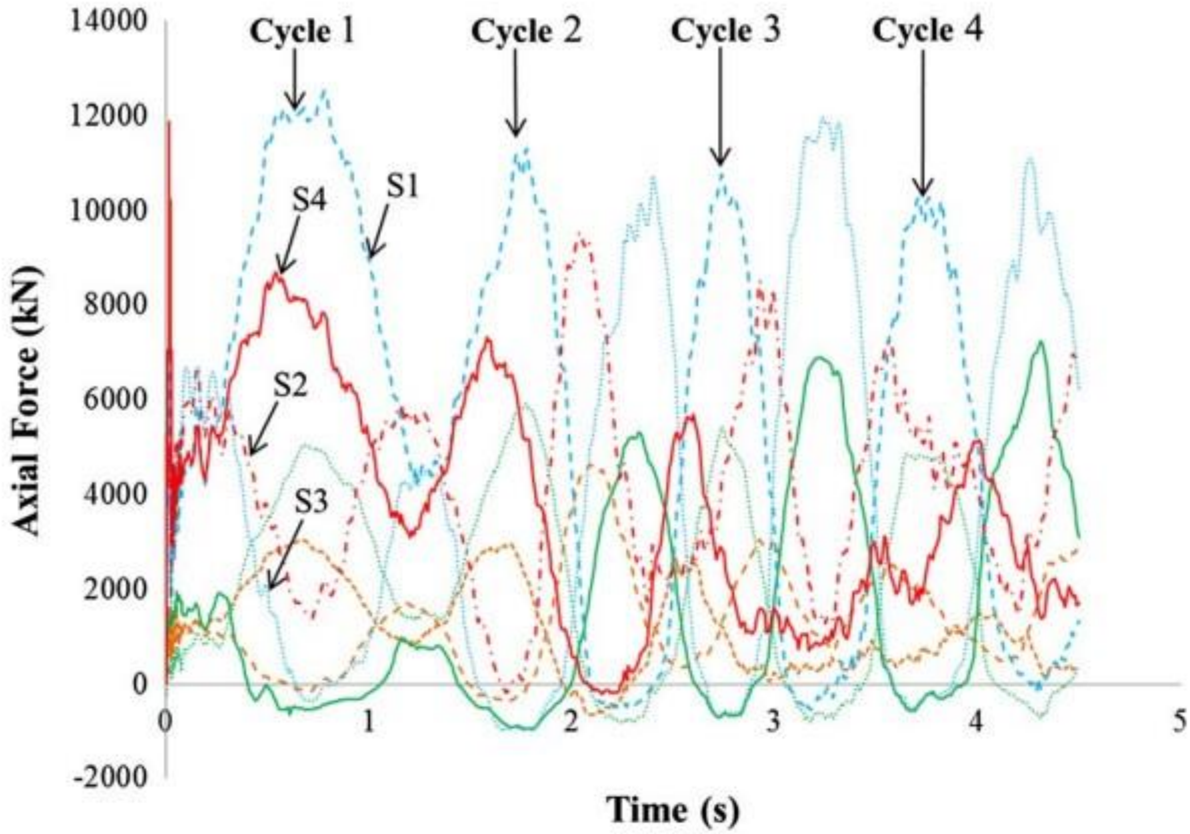

Fig. 16. Shear Wall Cyclic Dynamic Response as a Function of Time (4x4 SW)

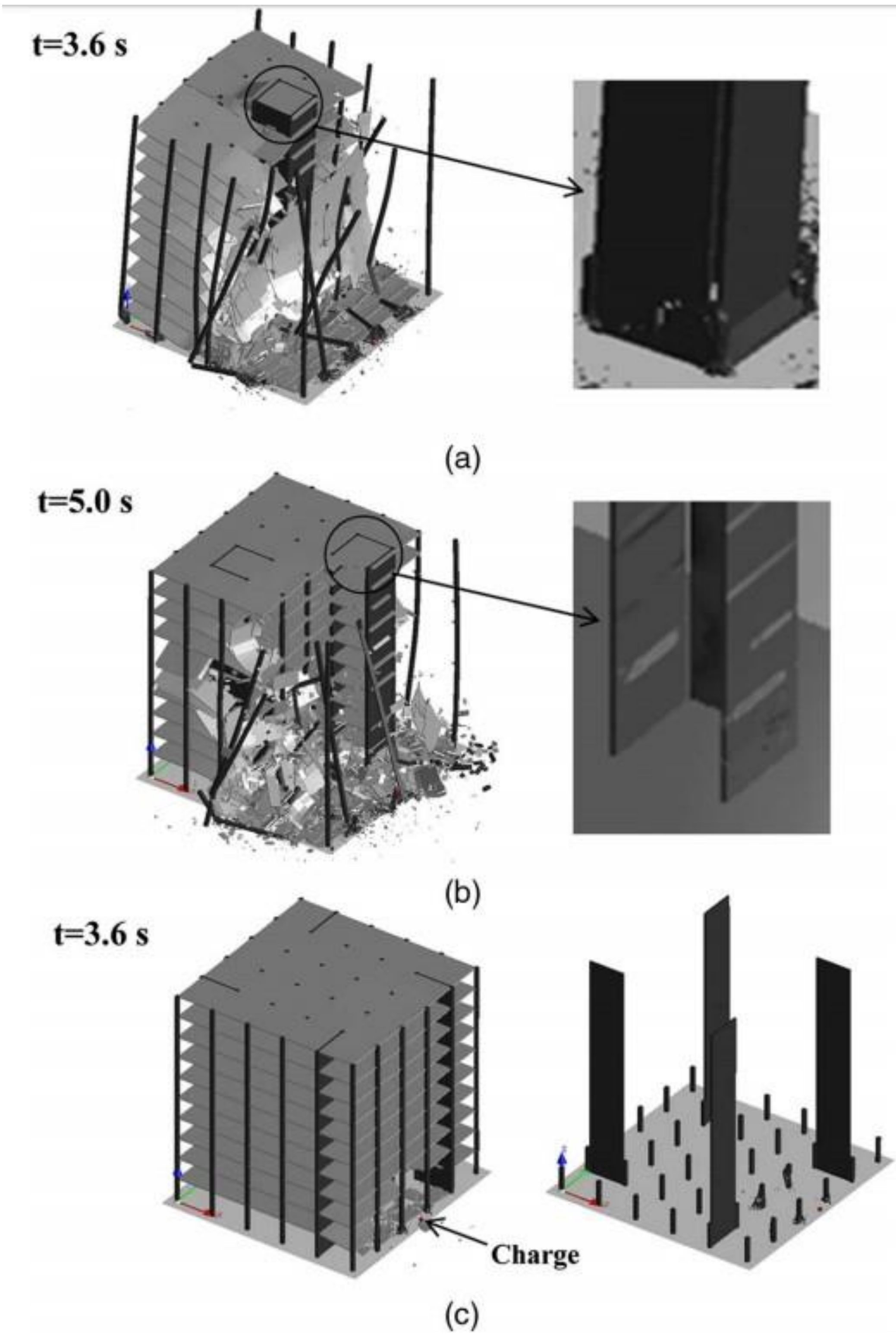

Fig. 17. Response of 4x4 Shear Wall Structure: (a) 3 Stories; (b) 6 Stories; (c & d) 10 Story

Alternate Shear Wall Configurations

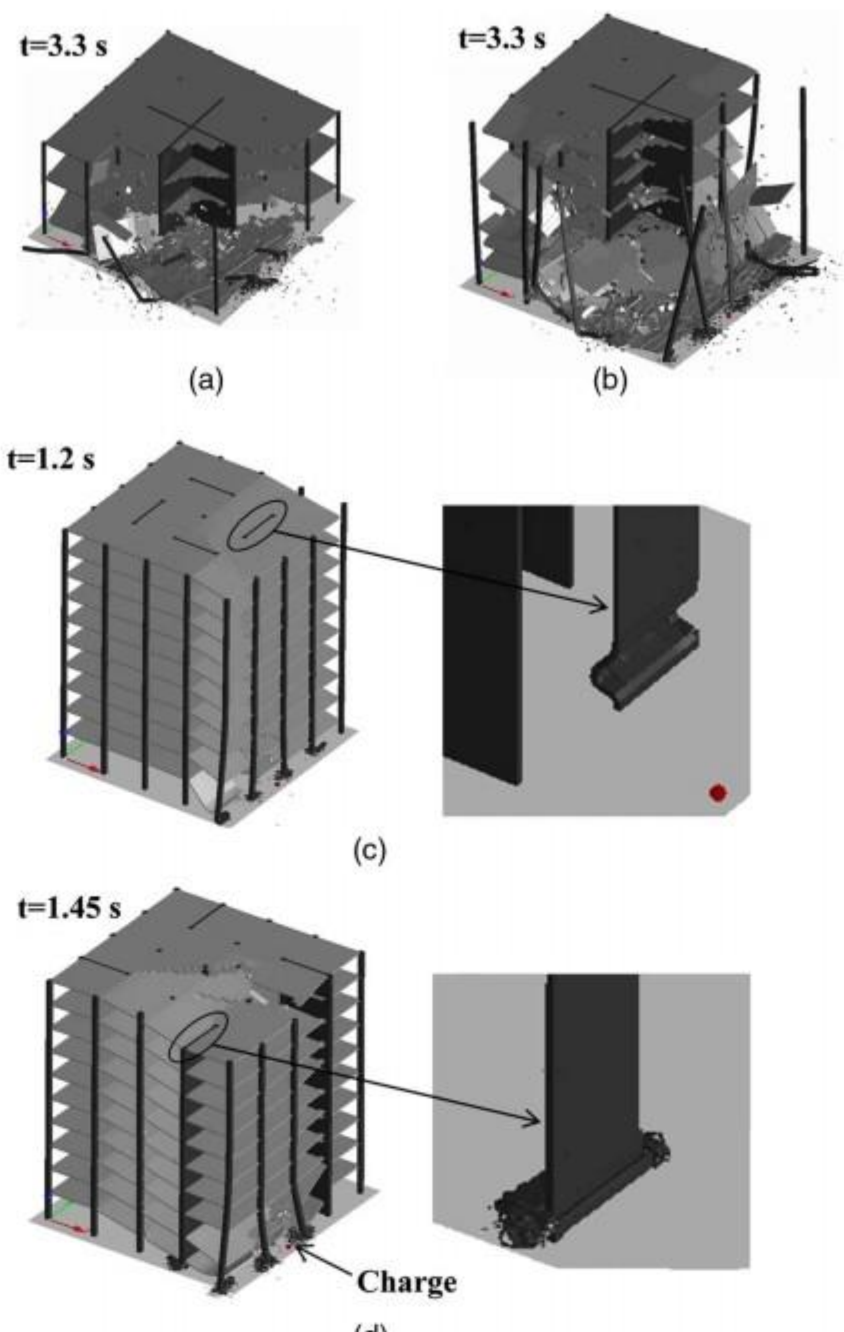

Fig. 18. Response of 5x5 Shear Wall Structures

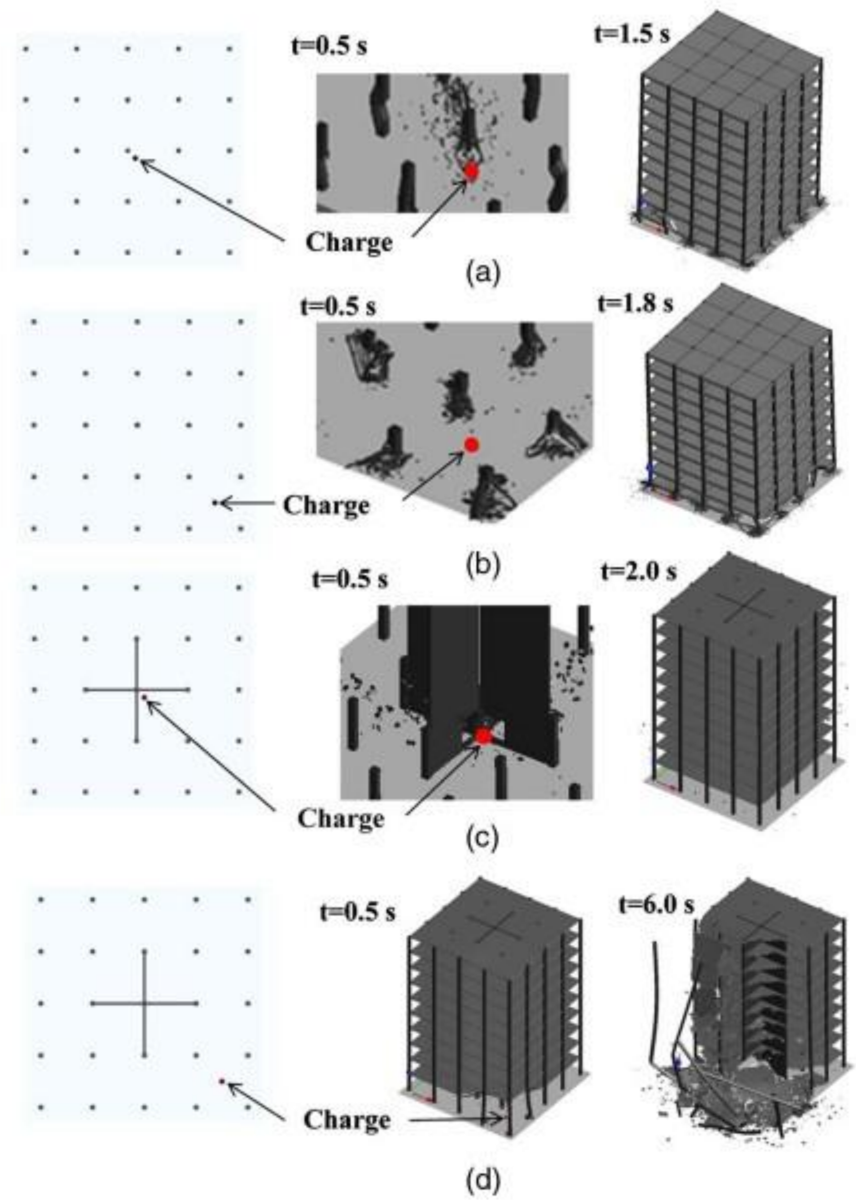

Fig. 19. Internal Blast Responses of 4x4 MRF and SW Structures